PAPER • OPEN ACCESS

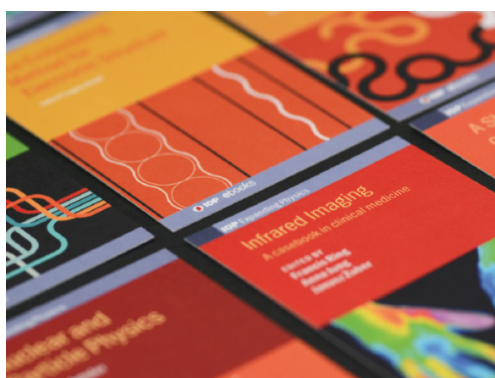# Enhanced radio-frequency performance of niobium films on copper substrates deposited by high power impulse magnetron sputtering

View the article online for updates and enhancements.

Enhanced radio-frequency performance of niobium films on copper substrates deposited by high power impulse magnetron sputtering

M Arzeo[1,2,*] , **F Avino**[1,3] , **S Pfeiffer, G Rosaz**[1] , **M Taborelli**[1]**, L Vega-Cid**[1]
and W Venturini-Delsolaro[1]

[1] European Organization for Nuclear Research (CERN), 1211 Geneva 23, Switzerland
[2] SeeQC-EU srl, Via dei due Macell 66, 00187, Roma, Italy
[3] Ecole Polytechnique Fédérale de Lausanne (EPFL), Swiss Plasma Center (SPC), Lausanne, Switzerland

E-mail: marzeo@seeqc.com

CrossMark

Abstract
We present a study of radio frequency properties of niobium films deposited on copper by two
different approaches based on High Power Impulse Magnetron Sputtering, namely with a DC
voltage biased substrate and with bipolar target voltage. Such approaches enable the synthesis
of dense superconducting (SC) layers. The SC radio frequency losses of these films are
characterized as a function of the applied RF magnetic field using a dedicated calorimetric
method. We report on a significant reduction of the Q-slope phenomenon and the residual
surface resistance in the characterized films, achieving similar values as those obtained on bulk
niobium surfaces qualified with the same technique. Our results pave the way towards the
realization of Nb/Cu coated accelerating cavities featuring a surface resistance 2–3 times lower
than the state-of-the-art values at working frequencies of 400 and 800 MHz, making this
technology even more appealing for future particle accelerators and colliders.

Supplementary material for this article is available online

Keywords: HiPIMS, SRF cavities, Nb thin film, Superconducting surface resistance,
Q-slope issue

(Some figures may appear in colour only in the online journal)

1. Introduction

Proton and electron accelerators are not only essential for fundamental studies in particle and high energy physics but also in different disciplines as biology, chemistry, solid-state physics [1], and medicine [2]. Advances in superconducting (SC) technology have always been beneficial for the realization of accelerating machines. In particular, the use of superconducting radio frequency (SRF) accelerating cavities has allowed to significantly improve the accelerators performance and to reduce the costs [3].

Bulk niobium SRF cavities are nowadays crucial for both electron and proton accelerators, which are respectively used for the generation of x-rays (e.g. European x-ray free electron laser—XFEL facility in Hamburg [4]), and for neutron spallation sources (e.g. European Spallation Source—ESS in Lund [5]). In fact, they have enabled the production of

---

* Author to whom any correspondence should be addressed.

electron/proton pulses with unprecedented intensity, quality and temporal structure. A real challenge is to satisfy the demand of continuous wave operation and high repetition rates to obtain even higher beam currents. To achieve such specifications, researchers in the field are currently trying to push the performance of bulk Nb RF cavities to their theoretical limits. Limitations can originate both from intrinsic properties of these objects and from environmental variables, such as cooling conditions or the effectiveness of the magnetic shielding around the cryostat. Therefore, to obtain the highest performance, a deep knowledge of the working behavior of the specific cavity, a proper monitoring and a good control of the environment are necessary.

In the search for a reduction in power consumption and for the achievement of larger-accelerating gradients, different alternatives are explored. In spite of the lower accelerating gradients which can be achieved, the niobium film on copper technology (Nb/Cu) represents one of the possible solutions, providing several advantages over the bulk Nb. It guarantees a reduction of the fabrication costs, a better thermal stability at cryogenic temperatures and a lower sensitivity to the ambient magnetic field [6]. Nb/Cu SRF cavities have been already successfully employed for circular colliders as the large electron–positron (LEP) collider [7] and the large hadron collider (LHC) [8], or linear accelerators like the High Energy and Intensity—Isotope mass Separator On-Line facility [9] at CERN or the Alpi accelerator at the LNL of Legnaro. Despite its advantages, this technology still exhibits a behavior known as 'Q-slope' resulting in a degradation of the quality factor of the cavity when increasing the accelerating voltage. This phenomenon is a direct consequence of the increase in the thin-film surface resistance when the latter is exposed to increasing surface magnetic field. At the beginning of this technology, the Nb films were deposited by DC magnetron sputtering (DCMS), as was the case for LEP [10] and LHC [11]. Since then, remarkable efforts have been done to improve the sputtering process as it was known that there is a direct impact on the RF performance [12, 13]. A potential cause of the 'Q-slope' has been identified in the shape of the cavities, that leads to off-normal impinging angle of the sputtered species during the coating process [14]. This induces porosities in the film and degrades its overall SC performances. In this study, we investigate a coating technique known as high power impulse magnetron sputtering (HiPIMS) allowing for the production of metal ions that can be accelerated toward the substrate [15] to densify the growing thin film [16, 17]. Experimental results indicate that this coating technique can provide residual surface resistance at the state-of-the-art for Nb/Cu films. At the same time, a significant mitigation of the 'Q-slope' is observed, with a shallow dependence of the surface resistance as a function of the peak magnetic field in the common operation range of the accelerating voltage.

2. Coating technique and film properties

The coating setup consists of a cylindrical cathode of 45 mm external diameter made out of pure niobium having a residual resistivity ratio of 300. The magnetic field is provided by a

Table 1. Summary of the two coating techniques parameters used in this study.

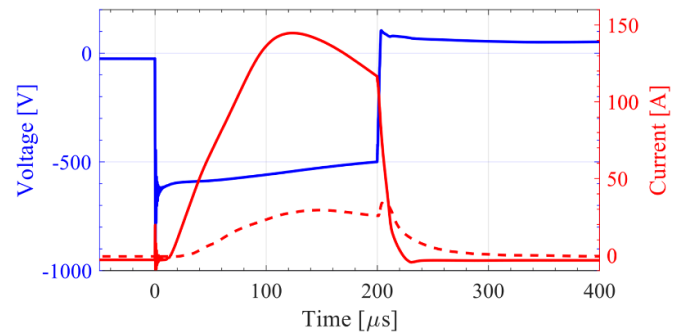| Parameter	Coating technique	
	HiPIMS + BS	HiPIMS + PP
Main pulse duration (μs)	200	30
Frequency (Hz)	100	1000
Average power (kW)	1.2	1
Peak current (A)	150	100
Bias voltage (V)	$-25/-50$	0
Positive pulse duration (μs)	N/A	200
Positive pulse delay (μs)	N/A	4
Positive pulse voltage (V)	N/A	80
Sputtering gas	Kr	Ar
Sputtering pressure (mbar)	2.3×10^{-3}	7×10^{-3}
Coating temperature (°C)	150	150
Coating duration (h)	6	6

Figure 1. In blue, the applied cathode voltage pulse for HiPIMS + BS. In red, the corresponding current wave-forms of the cathode (continuous line) and at the substrate (dashed line).

50 mm long and 30 mm in diameter NdFeB magnet inserted in the cathode. The sample is placed at a distance of 80.5 mm from the cathode in order to reproduce the location of a 1.3 GHz SRF cavity's equator. A detailed description of the coating apparatus is given in the supplemental material (available online at stacks.iop.org/SUST/35/054008/mmedia). The chamber is pumped down to a pressure of about 1×10^{-7} mbar. A bakeout is performed over 48 h at 200 °C after which the coating chamber and the sample are kept at 150 °C while the pumping station is cooled down to room temperature. A base pressure of 5×10^{-10} mbar is reached prior to coating. Two samples are coated using HiPIMS in two different configurations: the first (HiPIMS + BS) with the application of a bias to the substrate, the second (HiPIMS + PP) with a positive voltage pulse applied at the target during the afterglow keeping the substrate at ground potential. A comprehensive summary of the experimental parameters is given in table 1 with the corresponding voltage and current wave-forms shown in figures 1 and 2.

The supplementary material details the samples preparation prior to coating.

After RF testing, the two samples are characterized by x-ray fluorescence in order to evaluate the films thickness. The HiPIMS + BS and HiPIMS + PP films are 5.9 ± 0.2 μm and 4.2 ± 0.3 μm thick, respectively. The samples are
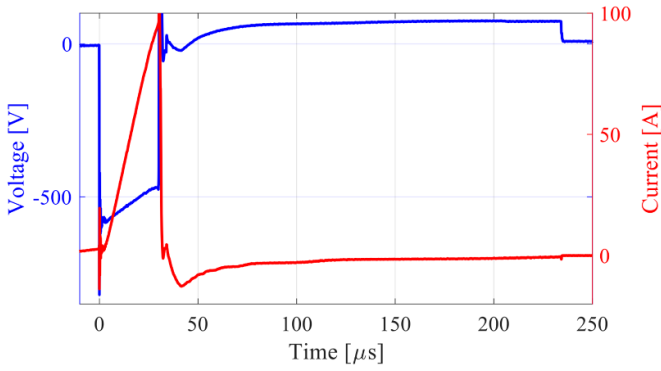
Figure 2. In blue, the applied cathode voltage pulse for HiPIMS + PP. In red, the corresponding current wave-form of the cathode.
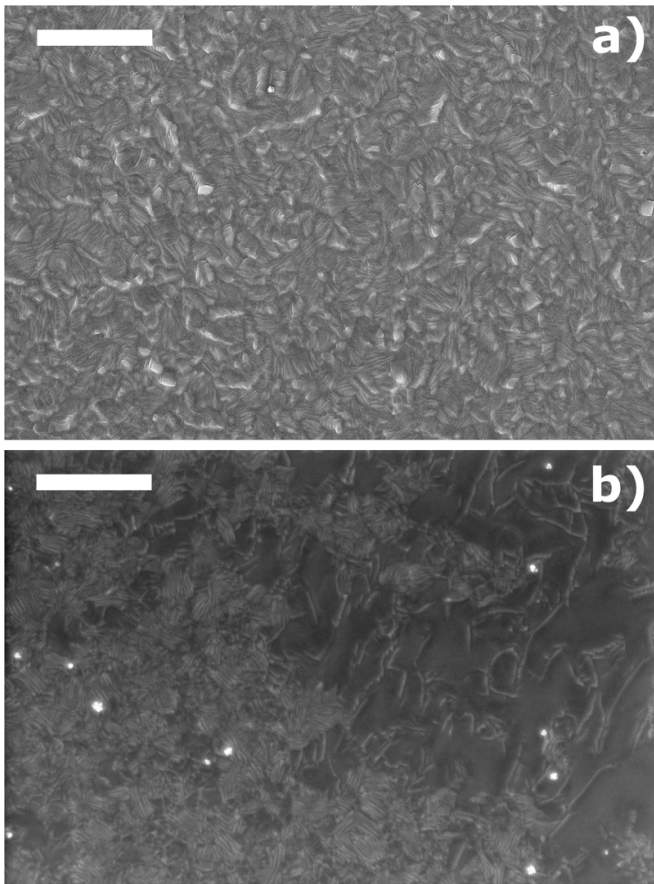

Figure 3. SEM top views of a niobium film coated by means of (a) HiPIMS + BS and (b) HiPIMS + PP. The scale bars represent 2 μm length.

Figure 4. FIB cross-sections of samples coated, using similar parameters as for the QPR resonators, using (a) HiPIMS + BS and (b) HiPIMS + PP techniques. The scale bars represent 2 μm length.

Table 2. Material parameters extracted from XRD analysis and the calculated dislocation density for the two elaborated Nb films.

Parameter	HiPIMS + BS	HiPIMS + PP
Crystallite size (nm)	91	54
Microstrain	0.00204	0.00268
Lattice parameter (Å)	3.30053	3.30101
Dislocations density (m^{-2})	2.7×10^{14}	6×10^{14}

also characterized by scanning electron microscopy (SEM) as shown on figure 3. The film surface looks very similar, with strongly faceted crytallites. The coating performed using HiPIMS + PP (figure 3(b)) exhibits a slightly smoother surface. Samples coated in similar conditions as the quadrupole resonator (QPR) were further analyzed by x-ray diffraction as well as by performing SEM cross-section observation after focused ion-beam (FIB) milling. The cross sections are presented in the figure 4. The average grain size at the top layer
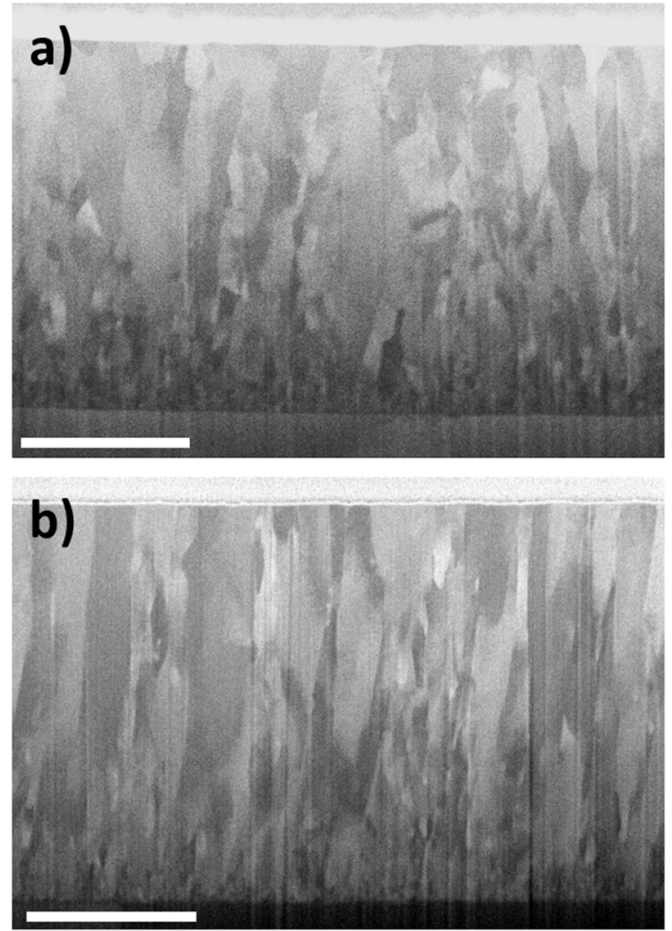
surface was extrated from the pitctures and a similar value of about 390 nm was found for both layers.

Using x-ray diffractograms we performed a full Rietveld analysis of the data using MAUD software [18]. From this analysis we extracted the crystallites size (D), micro-strain (ε) and lattice parameter (a). We then evaluated the dislocation density at the film surface expressed as:

$$\rho_D = 2\sqrt{3}\frac{\langle \varepsilon^2 \rangle^{1/2}}{D \times b} \tag{1}$$

where ρ_D is the dislocation density and b is the burger vector expressed as $\frac{a\sqrt{3}}{2}$ (m) for BCC materials.

The fitted and calculated data are summarized in table 2.

One can first notice that the crystallites size is much smaller than the grain size and thus most likely to be the driving parameters regarding the defect density such as dislocations. Both films exhibit lattice parameter slightly higher than the bulk Nb which implies a compressive residual stress in the layers, as is usually observed for thin films elaborated by physical vapor deposition [19]. Finally, we notice that both coating techniques lead to films having a high density of dislocations in the range of 10^{14} m^{-2} with an even higher value for HiPIMS + PP by more than a factor of 2. We discuss the potential effect of these defects onto the RF performance of the elaborated layers in section 4. It thus appears that despite the very different process parameters used for the elaboration of the two films the surface roughness and grain sizes remain qualitatively comparable. However, the dislocation density clearly appears to differ and may further impact the SRF behavior.

3. RF measurement and analysis methodologies

The CERN QPR is used for the characterization of the RF performance of small flat SC or metallic samples [20–22]. When the QPR is excited at its resonance modes, the RF currents circulating in the rods create an image current on the sample surface placed underneath. All the quadrupole modes (TE$_{21}$-like) up to 2 GHz are such that the RF fields exponentially decay in the 2 mm coaxial gap around the sample cylinder. The same applies for dipole modes (TE$_{11}$-like) below 1 GHz [23]. Therefore, one would expect that the power dissipation in the gap and, in particular, at the normal conducting end flange and copper joint, is negligible. However, as discussed later in this work and studied in more details in reference [24], this is not what is observed experimentally and extra dissipation in those normal conducting parts need to be taken into account. The current equipment allows for probing from the fundamental quadrupole mode up to the second harmonic ($f_0 \simeq 400$ MHz, $f_1 \simeq 800$ MHz and $f_2 \simeq 1200$ MHz). Such values are typical operation frequencies of most of the existing [25] and under-study accelerators (e.g. the RF systems of the Future Circular Collider (FCC) machines [26]). Indeed, this aspect represents a great value of the QPR. The RF properties of a SC coating, in fact, can be characterized in the whole frequency range of interest without the need of using substrate cavities of different size. For a more detailed description of the QPR and of its working principle, we refer to [23, 27] and references therein.

The surface resistance R_s of the SC material (film or bulk) is the actual physical quantity defining the cavity performance. Note that the Q_0 measured in a cavity is directly related to the average R_s of the SC film as follows:

$$Q_0 = \frac{G}{R_s}, \tag{2}$$

where G is a geometrical factor of the cavity that accounts for the electromagnetic field distribution. Therefore, measuring the R_s of the SC coating (or of a bulk sample) under investigation qualifies it for application in an accelerating cavity.

In this respect, the QPR is a very interesting tool as it allows to measure R_s as a function of the peak RF magnetic field B_{pk} on the sample surface at fixed temperature by means of an RF-DC compensation (or calorimetric) technique. In addition, the temperature dependence of R_s at a given RF field is also crucial. This is measured by keeping fixed B_{pk} while sweeping the temperature by means of the heater. In general, the full response to external RF electromagnetic field is described by the surface impedance $Z_s = R_s + i * X_s$, where the imaginary part X_s is known as surface reactance. While R_s is estimated as described above, the surface reactance X_s can be experimentally obtained from the measurement of the QPR cavity resonance frequency. In fact, within the London theory [28], if the temperature is not too close to T_c, one can write $X_s = 4\pi\omega\lambda$ [29]. Here $\lambda = \lambda_L \sqrt{\left(1 + \frac{\pi\xi_0}{2l}\right)}$ is the effective penetration depth of the electromagnetic field inside the superconductor, with λ_L being the London penetration depth, and ξ_0 the BCS coherence length. The variation of the penetration depth $\Delta\lambda = \lambda(T) - \lambda(T_0)$, with T_0 a reference temperature, is directly proportional to the change of the resonance frequency $\Delta f = f(T) - f(T_0)$ as follows [23]:

$$\Delta\lambda = -\frac{G}{\pi\mu_0 f^2}\Delta f, \tag{3}$$

where G is the sample geometry factor that depends on the mode. The change in the resonance frequency Δf is measured by heating up the sample with the DC heater above the transition temperature, while tracking the mode resonance with a vector network analyzer (VNA). A comparison to theoretical models allows to determine the main SC parameters characterizing the material. In the optimization process of the Nb on Cu coatings, the knowledge of the values of critical material parameters is crucial. The mean-free-path l and other fundamental SC parameters that play an important role on both DC transport and RF performance, being strongly related to the microstructural quality of the Nb layer, can be extracted from the analysis of $Z_s(T)$. To analyze both $\Delta\lambda(T)$ and $R_s(T)$ data we use numerical solutions of the BCS formulation of the RF surface impedance Z_s of a superconductor in the anomalous skin depth regime. The RF response of a superconductor within the BCS framework was first derived by Mattis and Bardeen (MB) [30] using a perturbation approach, in the low field limit. In particular, the real component, representing the RF surface resistance of a BCS superconductor R_{BCS} is associated to thermally activated quasiparticles, whose density decreases exponentially with temperature. All the remaining loss mechanisms, which dominate at low temperature ($T \ll T_c$), are generally included in a temperature independent term R_{res}, and thus the surface resistance is decomposed as follows:

$$R_s(T) = R_{BCS}(T; \xi_0, \lambda_L, l, \Delta, T_c) + R_{res}, \tag{4}$$

where R_{res} is referred to as residual resistance. The BCS term R_{BCS} is a function of the temperature and depends on the coherence length ξ_0, the London penetration depth λ_L, the mean-free-path l, the SC gap Δ, and the T_c of the superconductor.

A numerical calculation of both the real and the imaginary components of the $Z_s(T)$ of a superconductor was introduced and implemented by Halbritter [31]. This method is commonly used to analyze data from bulk Nb cavities, by fixing both the values of $\xi_0 = 39$ nm and $\lambda_L = 32$ nm, and varying l and Δ as fitting parameters to be extracted [32, 33]. The critical temperature is estimated independently. As the values of ξ_0 and λ_L in the case of Nb on Cu coatings depend on the deposition conditions and cannot be set *a priori*, they also need to be included in the fitting routine. In this work, we follow the procedure described and demonstrated in [34]. Due to correlations among some of the SC parameters, different set of values could provide good agreement between data and theory. In order to prevent non-physical estimations, we search for a set of four fitting parameters that minimizes a combination of the chi-square χ_s^2 values from both $\Delta\lambda(T)$ and R_s (T) experimental data.

4. Results and discussion

The most important figure of merit of an SRF cavity is the dependence of the unloaded quality factor Q_0 with respect to the accelerating gradient E_{acc} at a fixed temperature of operation. The unloaded quality factor Q_0 describes the ability of the cavity to store electromagnetic energy U, and it depends on the power dissipated on the cavity walls P_c as follows: $Q_0 = \frac{\omega U}{P_c}$, with $\omega = 2\pi f$ the operation frequency. For an accelerating cavity both Q_0 and E_{acc} are directly related via a geometric factor, respectively, to the value of the surface resistance R_s (2) and the peak RF magnetic field B_{pk}. These are the physical quantities that we extract from the experiments performed with the QPR (see section 3). In the following, the RF performance of the investigated samples, as a function of both the field and the temperature for all three different accessible quadrupole modes, is presented and described.

First, we report on the study of the temperature dependence of both the real and the imaginary parts of the complex surface impedance Z_s of the investigated samples. In figure 5(a) we show the temperature dependence of $\Delta\lambda$ for the HiPIMS + BS coated sample, as obtained from the experimental measurement in transmission of the resonance frequency (400 MHz mode) via a VNA with 10 dBm input power. In figure 5(b), instead, we display the temperature dependence of the surface resistance of the same sample, measured at $B_{pk} \simeq 5$ mT for the three different QPR modes. All error bars in the reported Rs data are estimated as the standard deviation of repeated measurements ($N = 20$). The results as a function of the temperature for the other two samples (bulk Nb and HiPIMS + PP coated) are reported in the supplemental material.

The solid lines in figure 5 represent the best numerical fit of the presented data as described in the previous section. Here, we emphasize that the critical temperature can be obtained by fitting the curve in figure 5(a) to the Gorter-Casimir expression. While heating up the sample to cross the transition temperature, radial temperature gradients are generated as the
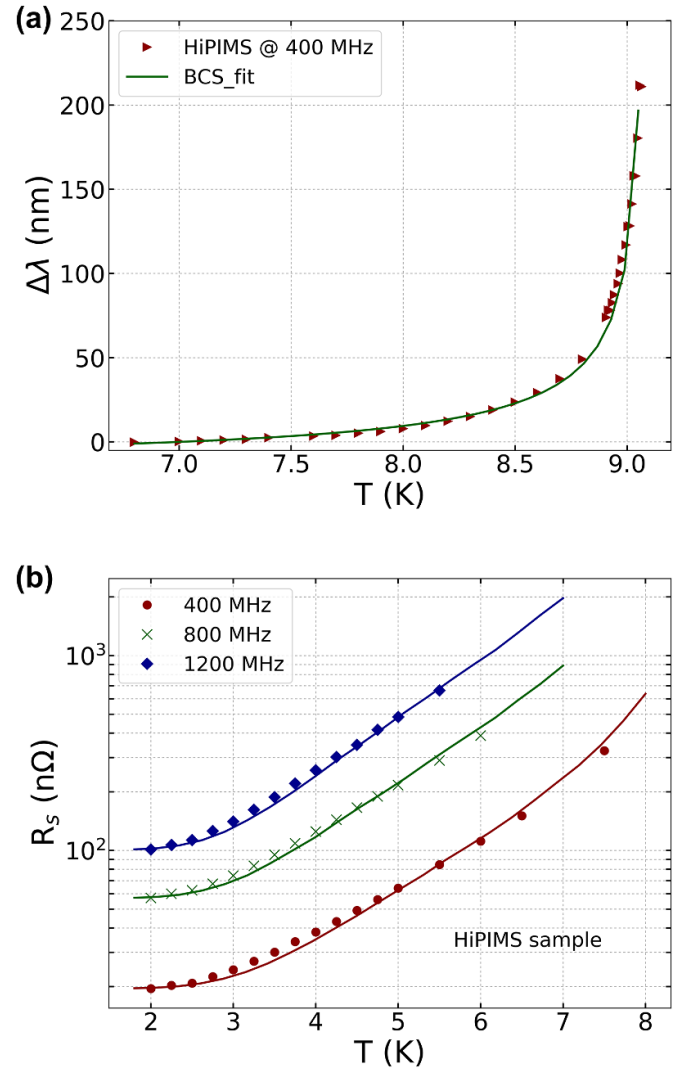

Figure 5. (a) Variation of the effective penetration depth $\Delta\lambda$ as a function of the sample temperature for the HiPIMS + BS coating. The solid line represents the best numerical fit to BCS theory. (b) Surface resistance R_s as a function of the sample temperature for the HiPIMS + BS coating for the three different quadrupole modes: 400 MHz (red), 800 MHz (green) and 1200 MHz (blue). Data are taken at $B_{pk} \simeq 5$ mT. The solid lines represent the numerical estimates of the BCS surface resistance, obtained with the same fitting parameters for all modes.

heater is in located at the center of the sample. The temperature sensor is not located in the hottest point, but at half radius approximately, which can lead to underestimations in the measurements. In the case of bulk Nb samples, due to the lower thermal conductivity, the gradients are expected to be higher. However, this has been studied with thermal simulations and they are expected to be negligible also for bulk Nb samples. The parameters obtained by applying the fitting procedure to data at 400 MHz are listed in table 3 for all the investigated samples. Note that the fit is made in order to get a consistent set of parameters fitting the results for all temperatures and frequencies of the measurements. It is important to emphasize that, provided a different R_{res} for the different

Table 3. BCS fitting parameters for the three different investigated samples.

Sample	l (nm)	ξ_0 (nm)	λ_L (nm)	$\frac{\Delta}{k_B T_c}$	T_c (K)
Bulk Nb	500 ± 125	33 ± 8	27 ± 7	2.1 ± 0.5	9.35
HiPIMS + BS	160 ± 40	28 ± 7	23 ± 6	2.3 ± 0.6	9.1
HiPIMS + PP	400 ± 101	32 ± 8	32 ± 9	2.3 ± 0.6	9.05

modes, the reported data scale in frequency in a very good agreement with what expected from BCS-MB.

All the samples are characterized by a long mean-free-path l, especially the bulk Nb, as expected from the large $RRR > 100$ of the raw material employed for its fabrication. This result demonstrates the high structural quality of the studied Nb coatings. This analysis provides crucial information on the coatings, which can be used together with the overall RF performance to effectively guide the choice of the best Nb deposition recipe to adopt in the future.

We now focus on the field dependence of the surface resistance R_s. In particular, in figure 6 we show the estimated R_s values versus the peak RF magnetic field B_{pk} at the fundamental frequency $f_0 = 400\,\text{MHz}$ and at two distinct sample's temperatures, namely $T = 2.5\,\text{K}$ (a) and $T = 4.5\,\text{K}$ (b).

At $T = 2.5\,\text{K}$ all the samples exhibit a linear field dependence of R_s within the measurement range, with a quite shallow slope (see figure 6(a)). At this temperature and frequency, the residual resistance R_{res} dominates over the BCS term, which would only account for 1–2 nΩ. Then, R_s can be approximated to $R_s \approx R_{res}$, with $R_{res} = R_{s0} + R_{s1} * B_{pk}$. The dashed straight lines represent the best fit. The obtained fitting parameters are listed in table 4, together with those extracted at the same temperature for the other two investigated frequencies. The relative data points, instead, are displayed in figure 4 of the supplemental material. The slope R_{s1} increases with frequency for the bulk Nb sample, whereas does not show a specific trend for the Nb films. In fact, HiPIMS + BS sample exhibits an inverse Q-slope at 800 MHz and then R_{s1} increases for the 1200 MHz frequency mode. Moreover, a decrease in R_{s1} value is instead observed for HiPIMS + PP sample. A deeper analysis of the observed inverse Q-slope would require a systematic study of all the samples, for all the accessible frequency modes and at peak magnetic fields lower than reported data. Such a study would be affected by larger uncertainties, intrinsic to the calorimetric technique in that field regime. It has also been observed that, at low fields, the results are sensitive to the external conditions, for example the temperature of the helium bath or the gap between the pole shoes and the sample. Moreover, a detailed analysis of the inverse Q-slope and its possible origin is beyond the main scope of this work. For all those reasons, the inverse Q-slope measured for HiPIMS + BS at 800 MHz has not been further investigated and could not be directly associated to physical properties of that specific sample. In the past years, several models to describe the RF field dependence of R_s at low temperature ($T \ll T_c$) have been proposed [35–37]. More specifically, an effort has been historically made to explain the physical
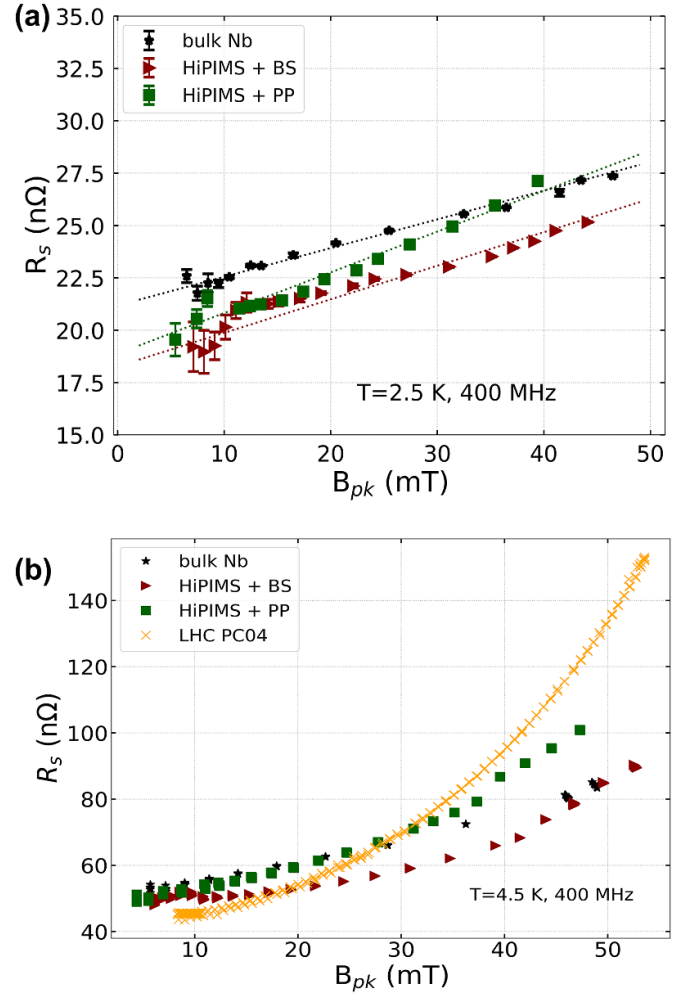

Figure 6. Surface resistance R_s as a function of the peak magnetic RF field B_{pk} at $f_0 = 400\,\text{MHz}$, $T = 2.5\,\text{K}$ (a) and $T = 4.5\,\text{K}$ (b) for the three characterized samples: bulk niobium (black stars), HiPIMS + BS coating (red triangles), HiPIMS + PP coating (green squares) and LHC PCO4 cavity (orange crosses). The dashed straight lines in (a) represent the best linear fit of the experimental data.

mechanisms behind the observed 'Q-slope' in Nb/Cu cavities. Although dedicated studies are needed to confirm the available models explaining the 'Q-slope', the data provided here could be exploited to benchmark those models. Furthermore, the fact that the coated samples show a surface resistance comparable to the bulk Nb one in terms of RF field dependence confirms that the Q-slope is not intrinsic to the thin films, but it can be overcome by having a better understanding of the coating processes and the operating environment.

Our data indicate that both HiPIMS samples are characterized by a weak linear field dependence, which compares to the bulk Nb within the limit of the employed measurement method. A direct comparison between bulk and films in absolute terms would require a deeper experimental investigation, which is beyond the scope of this work. Here, we highlight the experimental fact that the minimum of the R_s value is about 20 nΩ for all the investigated samples. Furthermore, the

Table 4. Linear fitting parameters for the three investigated samples at 2.5 K for the three different QPR modes.

Sample	400 MHz		800 MHz		1200 MHz	
	R_{s0} (nΩ)	R_{s1} (nΩ mT^{-1})	R_{s0} (nΩ)	R_{s1} (nΩ mT^{-1})	R_{s0} (nΩ)	R_{s1} (nΩ mT^{-1})
Bulk Nb	21.23 ± 0.04	0.136 ± 0.001	42.1 ± 0.1	0.32 ± 0.01	120.1 ± 0.3	0.69 ± 0.04
HiPIMS + BS	19.77 ± 0.05	0.109 ± 0.002	64.5 ± 0.2	$-0.38^{a} \pm 0.02$	101 ± 1	0.3 ± 0.1
HiPIMS + PP	18.87 ± 0.05	0.188 ± 0.003	37.5 ± 0.1	0.129 ± 0.007	n/a[b]	n/a[b]

[a] The R_s estimate for the 'HiPIMS + BS' sample at 800 MHz decreases up to about $B_{pk} \simeq 15$ mT (anti Q-slope), and then get flat up to the max measured RF field (see figure 3 in the supplemental material). Such results are reproducible, even between different cold tests.
[b] A hint of similar behavior is also observed for the 'HiPIMS + PP' sample at 1200 MHz. However, data are not presented and analyzed as affected by a faulty equipment. Here we point out that a surface resistance of about 250 nΩ was estimated at low field for this frequency mode.

lowest measurable R_s value increases with the frequency (see figure 5(b) and supplementary material). We attribute such experimental evidence to the QPR setup. In particular, we have identified, and are analyzing two possible limiting factors, which are not necessarily mutually exclusive. The first one is the possible presence of RF field in the coaxial gap around the sample's support, which interacts with highly dissipative non-SC parts. In fact, although the RF field from the quadrupole modes should be exponentially suppressed in that region [23], this might not be exactly the case because of possible asymmetries in the actual QPR geometry. This effect would be enhanced for higher frequency modes. Secondly, as described in section 3, each of the samples is welded to an outer niobium ring. The weld region could be characterized by a larger surface resistance as compared to the rest of the sample/coating, and thus contribute to an increase of the dissipated RF power. Indeed, the lowest R_s estimate for a bulk Nb sample via the QPR was obtained from a weld-free sample [13], a geometry which is therefore being considered for the upcoming experiments. At higher frequencies, the RF field is stronger at the sample's edge, where the weld is located, and hence an even larger contribution to P_{RF} is expected. In general, these two factors can also be combined to result in a larger estimate of the R_s of the samples. Moreover, to support the claim that the observed minimum R_s value has to be attributed to fundamental limitations of the QPR setup, HiPIMS coated Nb/Cu 1.3 GHz elliptical cavities with R_s down to $\simeq 10$ nΩ have been tested both at CERN and JLAB [36].

At $T = 4.5$ K a deviation from the linear field dependence is observed, indicating the contribution to R_s of the temperature dependent R_{BCS} component. This can be seen in figure 6(b), where the sample results for R_s versus B_{pk} are displayed in comparison to the bulk Nb one and to the curve obtained from an LHC-type cavity, named PC04, coated by DCMS and manufactured in the context of the LHC spare cavity production program [38]. The other observation that can be made from this plot is that the results from the HiPIMS samples are comparable to the bulk Nb one at this temperature, at least in the RF field range investigated with the QPR. The presented results demonstrate not only the feasibility of Nb/Cu coatings via energetic condensation techniques, but also the significant mitigation of the Q-slope that could be potentially achieved with respect to the classical DCMS technique, historically applied to the LHC cavities. This would eventually

result in an increase by a factor 2–3 of the unloaded Q-factor of 400 MHz LHC-like cavities as requested in the conceptual design report for the FCC study [26]. The next technological challenge lies in the transfer of this technique to a real-size cavity whose shape is more complex than a QPR sample. The latter is currently under investigation. It is eventually important to also point out that both the HiPIMS + BS and HiPIMS + PP techniques lead to similar RF performance despite the very different experimental parameters used, suggesting that the HiPIMS method may have a broad space parameter available for producing high-quality SRF films. The difference in the observed Q-slope between the HiPIMS + BS and HiPIMS + PP samples may arise from the difference in the dislocation density that has been shown to be more than twice higher in HiPIMS + PP film than those elaborated by HiPIMS + BS. An in-depth investigation is currently carried out to quantify the effect of these dislocations on the SC properties of films elaborated by HiPIMS.

5. Conclusions

Understanding the mechanism behind the Q-slope phenomenon in Nb/Cu cavities is a critical challenge in the SRF community. Already a mitigation of the performance degradation with increasing accelerating field represents a crucial breakthrough. The reported results indicate that making such a step is feasible by means of the HiPIMS coating technique, as a significant reduction of the Q-slope is demonstrated, even with different approaches. Within the accuracy limits of the experimental methodology employed, we observe a behavior of the surface resistance as a function of the peak magnetic field comparable to the bulk Nb sample. Future studies aiming at finding a direct correlation between the structural and morphological properties of Nb films made via HiPIMS with their RF performance might be the key to unlock this long-lasting technological issue.

Acknowledgments

Data availability statement

The data that support the findings of this study are available upon reasonable request from the authors.

ORCID iDs

M Arzeo ⬤ https://orcid.org/0000-0001-6558-4391
F Avino ⬤ https://orcid.org/0000-0002-6206-0960
G Rosaz ⬤ https://orcid.org/0000-0001-5987-128X

References

[1] Barbalat O 1994 Applications of particle accelerators *CAS - CERN Accel. Sch.: 5th Gen. Accel. Phys. Course* **23**

[2] Dosanjh M 2017 *From Particle Physics to Medical Applications* (Bristol: IOP Publishing) pp 2399–891

[3] Podlech H 2013 Superconducting versus normal conducting cavities *CAS - CERN Accel. Sch.: High Power Hadron Mach.* **151–70**

[4] Singer W *et al* 2016 Production of superconducting 1.3-GHz cavities for the European X-ray free electron laser *Phys. Rev. Accel. Beams* **19** 092001

[5] Bousson S, Darve C, Duthil P, Elias N, Molloy S, Reynet D and Thermeau J -P 2014 The ESS spoke cavity cryomodules *AIP Conf. Proc.* **1573** 665–72

[6] Benvenuti C, Calatroni S, Campisi I, Darriulat P, Peck M, Russo R and Valente A-M 1999 Study of the surface resistance of superconducting niobium films at 1.5 GHz *Physica* C **316** 153–88

[7] Sladen J 1998 Status of superconducting cavities in LEP *Part. Accel.* **60** 15–25 (https://cds.cern.ch/record/343059)

[8] Boussard D, Chiaveri E, Haebel E, Kindermann H, Losito R, Marque S, Rodel V and Stirbet M 1999 The LHC superconducting cavities *Proc. 1999 Particle Accelerator Conf.* pp 946–8

[9] Gerigk F 2018 Superconducting RF at CERN: operation, projects, and R&D *IEEE Trans. Appl. Supercond.* **28** 3500205

[10] Benvenuti C, Bernard P, Bloess D, Cavallari G, Chiaveri E, Haebel E, Hilleret N, Tuckmantel J and Weingarten W 1991 Superconducting niobium sputter-coated copper cavity modules for the LEP energy upgrade *Particle Accelerator Conf., 1991. Accelerator Science and Technology* vol 2 pp 1023–5

[11] Bauer S, Diete W, Griep B, Peiniger M, Vogel H, Chiaveri E and Losito R 1999 Production of Nb/Cu sputtered superconducting cavities for LCH *Proc. 1999 Workshop on RF Superconductivity, (La Fonda Hotel, Santa Fe, New Mexico, USA)* (https://epaper.kek.jp/SRF99/papers/wep016.pdf)

[12] Delsolaro W V *et al* 2013 Nb sputtered quarter wave resonators for the HIE-ISOLDE *Proc. SRF 2013 (Paris, France)* (http://ipnwww.in2p3.fr/srf2013/papers/weioa03.pdf)

[13] Aull S, Junginger T, Knobloch J, Sublet A, Valente-Feliciano A -M, Venturini Delsolaro W and Zhang P 2015 On the understanding of Q-slope of niobium thin films *Proc., 17th Int. Conf. on RF Superconductivity (SRF2015) (Whistler, Canada, 13–18 September 2015)* p TUBA03 (https://accelconf.web.cern.ch/srf2015/papers/tuba03.pdf)

[14] Benvenuti C, Boussard D, Calatroni S, Chiaveri E and Tuckmantel J a 1997 Production and test of 352-MHZ niobium sputtered reduced beta cavities *Proc. 1997 Workshop on RF Superconductivity, (Abano Terme (Padova), Italy)* pp 1038–49 (https://accelconf.web.cern.ch/srf97/papers/srf97d25.pdf)

[15] Avino F, Sublet A and Taborelli M 2019 Evidence of ion energy distribution shift in HiPIMS plasmas with positive pulse *Plasma Sources Sci. Technol.* **28** 01LT03

[16] Helmersson U, Lattemann M, Bohlmark J, Ehiasarian A P and Gudmundsson J T 2006 Ionized physical vapor deposition (IPVD): a review of technology and applications *Thin Solid Films* **513** 1

[17] Avino F, Fonnesu D, Koettig T, Bonura M, Senatore C, Perez Fontenla A, Sublet A and Taborelli M 2020 Improved film density for coatings at grazing angle of incidence in high power impulse magnetron sputtering with positive pulse *Thin Solid Films* **706** 138058

[18] Lutterotti L 2010 Total pattern fitting for the combined size-strain-stress-texture determination in thin film diffraction *Nucl. Instrum. Methods Phys. Res.* B **268** 334–40

[19] Russo R and Sgobba S 1997 Influence of the coating temperature on niobium films *Proc. 1997 Workshop on RF Superconductivity, (Abano Terme (Padova), Italy)* p SRF97D11 (https://accelconf.web.cern.ch/srf97/papers/srf97d11.pdf)

[20] Calatroni S *et al* 2019 Cryogenic surface resistance of copper: investigation of the impact of surface treatments for secondary electron yield reduction *Phys. Rev. Accel. Beams* **22** 063101

[21] Keckert S, Kleindienst R, Kugeler O, Tikhonov D and Knobloch J 2021 Characterizing materials for superconducting radiofrequency applications—a comprehensive overview of the quadrupole resonator design and measurement capabilities *Rev. Sci. Instrum.* **92** 064710

[22] Note that the QPR in [21] differs from the tool used in this work with respect to part of the design and in some measurement capabilities, e.g. the maximum magnetic field that can be reached. However, they share the same operating principle.

[23] Junginger T 2012 Investigation of the surface resistance of superconducting materials *PhD Thesis* Institute of Electronic Systems Warsaw University of Technology

[24] Keckert S *et al* 2021 Mitigation of parasitic losses in the quadrupole resonator enabling direct measurements of low residual resistances of SRF samples *AIP Adv.* **11** 125326

[25] Nassiri A *et al* 11 2015 History and technology developments of radio frequency (RF) systems for particle accelerators *IEEE Trans. Nucl. Sci.* **63** 1–1

[26] Benedikt M, Blondel A, Janot P, Mangano M and Zimmermann F 2020 Future circular colliders succeeding the LHC *Nat. Phys.* **16** 402–7

[27] Junginger T, Weingarten W and Welsch C 2012 Extension of the measurement capabilities of the quadrupole resonator *Rev. Sci. Instrum.* **83** 063902

[28] London F 1938 The λ-phenomenon of liquid Helium and the Bose-Einstein degeneracy *Nature* **141** 643

[29] Pippard A B 1950 The surface impedance of superconductors and normal metals at high frequencies V. Analysis of

experimental results for superconducting tin *Proc. R. Soc.* A **203** 195–210

[30] Mattis D and Bardeen J 1958 Theory of the anomalous skin effect in normal and superconducting metals *Phys. Rev.* **111** 412

[31] Halbritter J 1970 Comparison between measured and calculated RF losses in the superconducting state *Z. Phys.* **238** 466–76

[32] Checchin M, Martinello M, Grassellino A, Romanenko A and Zasadzinski J F 2017 Electron mean free path dependence of the vortex surface impedance *Supercond. Sci. Technol.* **30** 034003

[33] Maniscalco J T, Gonnella D and Liepe M 2017 The importance of the electron mean free path for superconducting radio-frequency cavities *J. Appl. Phys.* **121** 043910

[34] Miyazaki A and Venturini Delsolaro W 2019 Determination of the Bardeen-Cooper-Schrieffer material parameters of the HIE-ISOLDE superconducting resonator *Supercond. Sci. Technol.* **32** 025002

[35] Miyazaki A and Venturini Delsolaro W 2019 Two different origins of the *Q*-slope problem in superconducting niobium film cavities for a heavy ion accelerator at CERN *Phys. Rev. Accel. Beams* **22** 073101

[36] Junginger T 2015 Field dependent surface resistance of niobium on copper cavities *Phys. Rev. ST Accel. Beams* **18** 072001

[37] Gurevich A 2014 Reduction of dissipative nonlinear conductivity of superconductors by static and microwave magnetic fields *Phys. Rev. Lett.* **113** 087001

[38] Peauger F 2020 Test results of re-built LHC spare cavities *TESLA Technology Collaboration TTC2020* (https://indico. cern.ch/event/817780/contributions/3715414/attachments/ 1981758/3300529/2020_02_03-TTC-LHC-cavities- Peauger.pdf)